Ultrafast Phase Comparator for Phase-Locked Loop-Based Optoelectronic Clock Recovery Systems

Fausto Gómez-Agis, Leif Katsuo Oxenløwe, Sunao Kurimura, Cédric Ware, Hans Christian Hansen Mulvad, *Associate Member, IEEE*, Michael Galili, and Didier Erasme

***Abstract*—The authors report on a novel application of a $\chi^{(2)}$ nonlinear optical device as an ultrafast phase comparator, an essential element that allows an optoelectronic phase-locked loop to perform clock recovery of ultrahigh-speed optical time-division multiplexed (OTDM) signals. Particular interest is devoted to a quasi-phase-matching adhered-ridge-waveguide periodically poled lithium niobate (PPLN) device, which shows a sufficient high temporal resolution to resolve a 640 Gbits OTDM signal.**

***Index Terms*—Clock recovery (CR), nonlinear optics, optical communication, optical phase matching, optical signal processing, optical time division multiplexing (OTDM), optoelectronic phase-locked loop (OEPLL), periodically poled lithium niobate (PPLN).**

I. Introduction

ALTHOUGH current optical networks based on time-division multiplexing (TDM) are quite mature, the increasing demand on bandwidth to satisfy services, such as digital television, telephony, video on demand, and internet, requires upgrading of the transmission capacity of existing communication links. This implies that different functionalities such as clock recovery (CR) needed for demultiplexing or for channel adding–dropping, must also be upgraded. To carry it out, all-optical and optoelectronic techniques have been investigated; notably optoelectronic phase-locked loops (OEPLLs) by replacing the upfront phase comparator by a nonlinear optical device. Systems using four-wave mixing or crossgain modulation in semiconductor optical amplifiers (SOAs) [1]–[5], electro-absorption modulators (EAM) [6], [7], two-photon absorption in a photodetector [8], or passive mode-locked lasers [9], [10] have been demonstrated. Recently, similar systems incorporating a quasi-phase-matched (QPM) adhered-ridge-waveguide (ARW) periodically poled lithium niobate (PPLN) device, have shown an outstanding performance as well [11]–[13].

QPM waveguide devices based on PPLN have attracted much attention being tailored in order to demonstrate different applications, for example, blue/UV light generation, all-optical gates with arbitrary wavelength conversion [14], [15], monolithic optical time-division multiplexers (OTDM) [16], [17], and chromatic-dispersion compensation in longhaul division-wavelength dense multiplexing (DWDM) systems by means of phase conjugation [18]–[20].

Due to the degraded nonlinearity and low stability for long-term operation in ordinary PPLN waveguides, ARWs in $LiNbO_3$ have been studied in [21], [22]. Their advantages as per [22] reside in the symmetric mode profiles and strong light confinement due to a step index profile. In addition, no degradation of the nonlinear coefficient or any photorefractive damage, which is mitigated by heating up the waveguide at lower temperatures than employed in conventional PPLN waveguides, is exhibited. Hence, a high conversion efficiency, low optical powers of operation, and stability using ARW in PPLN waveguide devices are obtained.

A recent explored application based on ARW–PPLN devices is that of a phase comparator in an OEPLL serving for determining the phase difference (time delay) between the envelopes of two optical signals. This information provided at the output of the phase comparator is further used for locking purposes in an OEPLL. Although experimental results have verified that a phase comparator based on ARW–PPLN devices exhibits no patterning effects and a sufficient high temporal resolution to resolve a 640 Gbit/s OTDM signal [12], [13], investigations on this application are not reported in the literature. In this paper, we present the experimental procedure employed for characterizing an optical phase comparator based on PPLN, including an explanation of the physical process behind its operation.

The content of the paper is structured as follows. Section II explains the principle of operation of an OEPLL and its dependence on a phase comparator to accomplish CR. Section III describes the physical process behind a phase comparator based on PPLN by an experimental demonstration on OTDM signals (in Section IV) at 160, 320, and 640 Gbit/s. In Section V, the phase comparator's sensitivity is derived and incorporated to a PLL transfer function to obtain that of an OEPLL. Finally, conclusions are drawn from the experimental results.

Manuscript received June 10, 2008; revised October 13, 2008. First published April 17, 2009; current version published July 01, 2009. This work was supported by the e-Photon/ONe+ and BONE-project ("Building the Future Optical Network in Europe") a Network of Excellence funded by the European Commission through the 7th ICT-Framework Programme and the cooperative actions COST 291 and 288, and partially supported by the National Institute of Information and Communication Technology, Japan. The work of F. Gómez-Agis was supported by a scholarship from CONACyT—Mexico.

F. Gómez-Agis, C. Ware, and D. Erasme are with Institut TELECOM, TELECOM ParisTech, LTCI CNRS, Communications and Electronics Department, F-75634 Paris Cedex 13, France (e-mail: fausto.gomez@telecom-paristech.fr; cedric.ware@telecom-paristech.fr; didier.erasme@telecom-paristech.fr).

L. K. Oxenløwe, H. C. Hansen Mulvad, and M. Galili are with Department of Photonics Engineering, DTU Fotonik, Technical University of Denmark, DK-2800 Lyngby, Denmark (e-mail: lkox@fotonik.dtu.dk; hchm@fotonik.dtu.dk; mgal@fotonik.dtu.dk).

S. Kurimura is with National Institute for Materials Science, Tsukuba 305-0044, Japan (e-mail: kurimura.sunao@nims.go.jp).

Digital Object Identifier 10.1109/JLT.2008.2010957

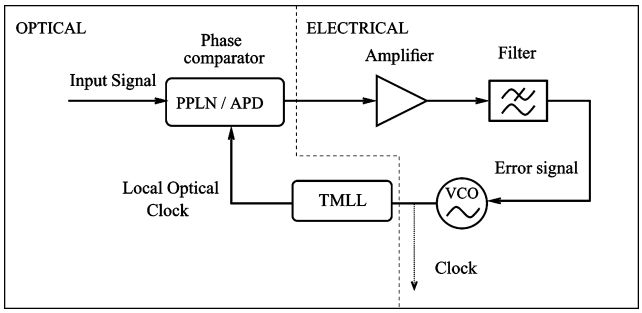

Fig. 1. Optoelectronic diagram for ultrahigh-speed clock recovery.

II. Phase Detector in the OEPLL

The OEPLL used as a CR unit is represented schematically in Fig. 1. It consists of a local optical clock driven by a voltage-controlled oscillator (VCO), a phase comparator, a loop filter, and optionally an amplifier.

The aim of the system is to adjust the frequency and phase of the *clock* to maintain it at a desired value which corresponds to that of the frequency and phase of the *input signal*. The latter is coupled together with the *local optical clock* into the PPLN whose output connected to a silicon avalanche photodetector acts as a phase comparator [23], thus generating an *error signal* as a function of the time delay (phase difference) between the envelopes of both signals. The optical clock consists of a tunable mode-locked laser (TMLL) generating optical pulses at the oscillation frequency of the VCO.

The low-pass filter reduces the amount of noise present in the error signal, damps the response of the OEPLL that copes with spurious changes in phase coming from its input, and sets the length requirements on the overall loop (acquisition time). When the desired value in the phase of the clock is attained, we say the clock is recovered or extracted.

III. $\chi^{(2)}$ Phase Comparator

A. Sum-Frequency Generation by Three-Wave-Mixing

In general, the phase-comparison task is carried out by electronic devices such as mixers or multipliers; however, CR of optical signals beyond 100 Gbit/s is currently not possible since electronics is not mature enough to function at these rates. Thus, optical techniques are preferred instead.

In the optical domain, optical frequencies can be mixed to generate new ones, like radio frequency (RF) mixers do in the electrical domain. This is possible by means of nonlinear optical processes such as three-wave-mixing (TWM) performed in media holding a nonlinear optical susceptibility of order 2, $\chi^{(2)}$. For example, the sum-frequency (SF) generation process, which consists in creating an optical frequency by the sum of two others, can be carried out in a PPLN waveguide by means of the QPM technique. This technique leads to a continuous buildup of the created optical frequency and provides a wide range of phase matching (tuning), thus allowing for interactions among any combination of wavelengths within the transparency range of the material employed.

In a PPLN device, the sign of the material's $\chi^{(2)}$ nonlinear coefficient is periodically reversed along an interaction distance in order to correct the phase mismatch between the interacting signals, which is caused by the dispersion in the $LiNbO_3$. This systematic phase-match correction allows for continuous buildup of the created signal. If uniform modulation along the waveguide is used, the period length will correspond to the wavelength where the PPLN performs second harmonic generation (SHG)—a special case of the SF-generation process where a single optical signal interacts with itself.

According to [24], [25], the power of the created optical signal by SF generation in a PPLN waveguide of length L can be written as

$$P_{\mathrm{SF}}(L) = P_{\mathrm{s}} P_{\mathrm{c}} \mathcal{K} L^2 \mathrm{sinc}^2[\Delta k_{\mathrm{Q}} L/2] \tag{1}$$

where $\mathcal{K}$ is the conversion efficiency independent of the length of waveguide, and P_{s} and P_{c} are the power of the interacting signals. P_{SF} is reduced in the presence of a nonzero quasi-phase-matching condition (effective wave vector mismatch) given by $\Delta k_{\mathrm{Q}} = \Delta k' - k_{\mathrm{m}}$. The variables $\Delta k' = |k_{\mathrm{SF}} - k_{\mathrm{c}} - k_{\mathrm{s}}|$ and $k_{\mathrm{m}} = 2\pi/\Lambda$ designate the phase-matching (PM) condition for the interacting signals in the medium and the wave vector associated with the modulated structure, respectively. $k_i = 2\pi n_i/\lambda_i (i = _{\mathrm{SF,c}}$, and $_{\mathrm{s}})$ defines the wave vectors associated with the interacting signals in the SF-generation process and n_i and λ_i, their respective indices of refraction and wavelengths. Finally, Λ represents the period of the modulated structure which can be modified to a particular requirement in order to satisfy the condition $k_{\mathrm{m}} = \Delta k'$ [24].

By conservation of energy, $\omega_{\mathrm{SF}} = \omega_{\mathrm{s}} + \omega_{\mathrm{c}}$, where $\omega_{\mathrm{SF}}, \omega_{\mathrm{s}}$, and ω_{c} are the optical frequencies of the interacting signals in the SF process must be satisfied. So the created optical signal, λ_{SF}, matches

$$\lambda_{\mathrm{SF}} = [\lambda_{\mathrm{s}}^{-1} + \lambda_{\mathrm{c}}^{-1}]^{-1} \tag{2}$$

where λ_{s} and λ_{c} represent, respectively, in the remainder of the paper, the input signal and the optical clock in an OEPLL. Finally, λ_{SF} will denote the wavelength of the error signal.

Although PPLN is among the fastest optical signal processing devices available today, when involving modulated optical signals, it presents speed limits set by the group-velocity mismatch (GVM) between the fundamental harmonic (FH) and the SHG [26], thus giving rise to the so-called effect of walkoff. That is, the SHG travels slower than the FH in the waveguide. The walkoff effect is of great importance, since the frequency components within the bandwidth of the optical envelops experience different group velocities, and the phase matching is partially achieved, resulting in a reduced SHG conversion efficiency and a distorted waveform of the generated signal.

Following the formalism employed in [27], we study the effect of the GVM on the SF-generation process when modulated optical signals are involved. So, the frequency-domain envelope of the created optical signal (error signal) can be written as

$$\tilde{A}_{\mathrm{SF}}(L,\Omega) = [\tilde{A}_{\mathrm{s}} * \tilde{A}_{\mathrm{c}}](\Omega)\tilde{\mathcal{H}}(\Omega) \tag{3}$$

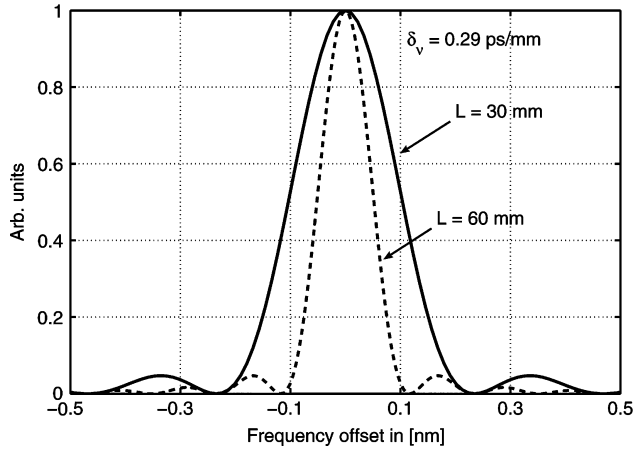

Fig. 2. $\bar{\mathcal{H}}$ trace for a given δ_v scaled by the waveguide length L. $\bar{\mathcal{H}}$ is traced as a function of the detuning frequency (in nm) from the nominal SF wavelength, $\lambda_{\rm SF}$. The width of function is reduced by a factor of two as the length of the waveguide increases by the same factor.

with

$$\tilde{\mathcal{H}}(\Omega) = \mathcal{K}L\,\mathrm{sinc}[(\Delta k_{\rm Q} + \Omega\delta_v)L/2] \tag{4}$$

where Ω designates the detuning frequency from the nominal SF optical frequency $\omega_{\rm SF}$, and $\delta_v = 1/v_{\rm SF} - 1/v_{\rm s}$ the GVM parameter, where $v_{\rm s}$ and $v_{\rm SF}$ are the group velocities for the input and the SF signal, respectively. The operator "$*$" indicates that a convolution operation is performed. $\tilde{\mathcal{H}}$ represents the transfer function of the PPLN waveguide that relates the spectrum of the SF envelope, represented by the variable $\tilde{A}_{\rm SF}$, to the spectrum of the convolution between the frequency-domain envelopes of the input signal and the optical clock, designated by $\tilde{A}_{\rm s}$ and $\tilde{A}_{\rm c}$, respectively. $\tilde{\mathcal{H}}$ can be viewed as a filter acting on the spectral components of the interacting signals, since it only depends on the dispersive properties and on the modulated nonlinear coefficient of the medium. The width of this filter function, denoted by $\Delta\Omega_g$, depends on the GVM parameter and scales inversely to the length of the waveguide. For example, (4) is evaluated for a given GVM, $\delta_v = 0.29$ ps/mm, and two different waveguide length values: $L = 30$ mm and $L = 60$ mm. A $\Delta k_{\rm Q} = 0$ condition has also been assumed. As depicted in Fig. 2, the width of the function is reduced by a factor of 2 as the length of the waveguide increases by the same factor.

B. Phase-Comparator Operation on OTDM Signals

The input to the OEPLL consists of an OTDM signal where multiple low-bit rate channels of data are interleaved in time to create an ultrahigh bit-rate channel whose repetition frequency, $f_{\rm s}$, is considered to be equal or close to N times the running frequency of the optical clock, $f_{\rm c}$. In the remainder of this paper, the bit rate of an individual channel will be referred to as the base rate of the OTDM signal.

To perform a phase-comparison operation at the scale of $f_{\rm s}$, the Nth harmonic of the optical clock must be considered. To demonstrate this, we assume that both the optical clock and the data signal, being quasi-periodic, can be represented by their Fourier series, which can converge to a cosine series if the pulses are symmetrical. The data input and the optical clock time-domain amplitude-envelopes can be written as

$$A_{\rm s}(t) = A_{{\rm s},0} + m_1 \sum_{k=1}^{\infty} A_{{\rm s},k} \cos[k(\omega_{f_{\rm s}} t + \Phi_1)] \tag{5}$$

$$A_{\rm c}(t) = A_{{\rm c},0} + m_2 \sum_{l=1}^{\infty} A_{{\rm c},l} \cos[l(\omega_{f_{\rm c}} t + \varphi_2)] \tag{6}$$

where $A_{{\rm s},k}$ and $A_{{\rm c},l}$ represent the amplitudes of the interacting signals, and $\Phi_1 = N\varphi_1$ and φ_2, their respective phases. $\omega_{f_{\rm s}}$ and $\omega_{f_{\rm c}}$ are the repetition frequencies $f_{\rm s}$ and $f_{\rm c}$ expressed in rad/s. φ_1 designates the phase of an individual channel and $|m_i \leq 1|$ ($i = 1$ and 2), a dimensionless scale factor to control the contrast of the modulations. Substituting the Fourier transforms of (5) and (6) in (3) we have that

$$\begin{aligned}
[\tilde{A}_{\rm s} * \tilde{A}_{\rm c}](\Omega) = {} & A_{{\rm s},0}A_{{\rm c},0}\delta[\Omega] \\
& + m_2 \sum_{l=1}^{\infty} \frac{A_{{\rm s},0}A_{{\rm c},l}}{2} \\
& \times (\beta_2^{+}\delta[\Omega + l\omega_{f_{\rm c}}] + \beta_2^{-}\delta[\Omega - l\omega_{f_{\rm c}}]) \\
& + m_1 \sum_{k=1}^{\infty} \frac{A_{{\rm c},0}A_{{\rm s},k}}{2} \\
& \times (\beta_1^{+}\delta[\Omega + k\omega_{f_{\rm s}}] + \beta_1^{-}\delta[\Omega - k\omega_{f_{\rm s}}]) \\
& + \sum_{k=1}^{\infty}\sum_{l=1}^{\infty} m_1 m_2 \frac{A_{{\rm s},k}A_{{\rm c},l}}{4} \\
& \times (\beta_1^{+}\beta_2^{+}\delta[\Omega + k\omega_{f_{\rm s}} + l\omega_{f_{\rm c}}] \\
& + \beta_1^{+}\beta_2^{-}\delta[\Omega + k\omega_{f_{\rm s}} - l\omega_{f_{\rm c}}] \\
& + \beta_1^{-}\beta_2^{+}\delta[\Omega - k\omega_{f_{\rm s}} + l\omega_{f_{\rm c}}] \\
& + \beta_1^{-}\beta_2^{-}\delta[\Omega - k\omega_{f_{\rm s}} - l\omega_{f_{\rm c}}])
\end{aligned} \tag{7}$$

where $\beta_1^{\pm} = \exp[\pm ik\Phi_1]$ and $\beta_2^{\pm} = \exp[\pm il\varphi_2]$. Assuming a QPM condition $\Delta k_{\rm Q} = 0$ with $k = 1$ and $l = N$, and a photodetection bandwidth to several tens of MHz, we can verify that: 1) if there is a small offset between $f_{\rm s}$ and the nearest harmonic of the clock signal $Nf_{\rm c} \approx f_{\rm s}$, $P_{\rm SF}$ (the power of the error signal) will bear a frequency component $f_{\rm out} = |f_{\rm s} - Nf_{\rm c}| = |\Delta f|$; and 2) if the frequency detuning Δf is null $f_{\rm out} = 0$; namely, $Nf_{\rm c} = f_{\rm s}$, $P_{\rm SF}$ will be constant with a varying magnitude in the function of the time delay between the input signal and the optical clock, as indicated by the phase term products $M\beta_1^{+}\beta_2^{-}\delta[\Omega]$ and $M\beta_1^{-}\beta_2^{+}\delta[\Omega]$ where $M = m_1 m_2 (A_{{\rm s},k}A_{{\rm c},l}/4)$. The oscillating terms at $k \neq 1$ and $l \neq N$, and those at $f_{\rm s}$ and $2f_{\rm s}$ are filtered out.

The equation describing the nonlinear transfer characteristics of a $\chi^{(2)}$ phase comparator for sinusoidally modulated inputs is given by

$$P_{\rm SF} = P_0 + P_1\,\cos[\Psi_e] + p[\Psi_e] \tag{8}$$

where $\Psi_e = N\varphi_e$ and $\varphi_e = \varphi_1 - \varphi_2$ represent the phase difference between the envelopes of the interacting signals scaled to the repetition frequencies $f_{\rm s}$ and $f_{\rm c}$, respectively. The variable P_0 designates the average optical power of the error signal,

and P_1 is its modulation index (or contrast) whose magnitude depends not only on the power of the spectral lines of the interacting signals associated with the repetition frequency at which the phase-comparison operation takes place, but also on the conversion efficiency for a given $\lambda_{\rm SF}$. Finally, $p[\Psi_e]$ denotes higher order terms with coefficients much smaller than P_1.

From (3), we observe that the filter function $\tilde{\mathcal{H}}$ acts on the resulting low-frequency variation term. Depending on the parameter $\Delta\Omega_g$, linked to the PPLN device length, $\tilde{\mathcal{H}}$ may or may not filter out the spectral line at the frequency detuning Δf. For example, for $L = 60$ mm, the maximum frequency detuning Δf that can be passed through $\tilde{\mathcal{H}}$ is $\sim$10 GHz, whereas for $L = 30$ mm, a $\Delta f\sim$20 GHz is allowed. In our particular case, the frequency variation of the error signal is lower than that, so that, the GVM is not an issue for this application.

Finally, the spectrum of (3), denoted by $S_{\rm SF}$, is of the form

$$S_{\rm SF}(\Omega) = S_{\rm sc}(\Omega)|\tilde{\mathcal{H}}(\Omega)|^2 \tag{9}$$

where $S_{\rm sc}$ represents $|\tilde{A}_{\rm s} * \tilde{A}_{\rm c}|^2$.

IV. Experimental Phase Comparator

A. ARW–PPLN Device

In the experiments to be described, we have employed a fiber-pigtailed and temperature-controlled ARW Mg-doped $LiNbO_3$ device in a fiber-pigtailed module that will be referred to as ARW–PPLN in the remainder of the paper. At 25°C, its SHG phase-matching curve peaks at 1565 nm ($\lambda_{\rm SF}\simeq$782.5 nm) with an approximately 1 nm bandwidth, as illustrated in its experimental SHG tuning curve in Fig. 3. A second phase-matching peak is present at 1562.8 nm ($\lambda_{\rm SF}\simeq$781.5 nm), whose presence could be due to some mechanical stress applied to the waveguide during the packaging process, resulting in a modification of the Λ parameter in some region of the waveguide. The normalized SHG conversion efficiency attained is about 350% $\rm W^{-1}$ in contrast to 125% $\rm W^{-1}$ obtained in a 90 mm long bare chip used in the experiments described in [23]. The ARW dimensions are $\simeq 8$ μm width, $\simeq 2.5$ μm height, and 30 mm long with a structure period $\Lambda = 17$ μm. For more details about its construction, please refer to [22].

The experimental wavelength range within which this particular device performs SHG, denoted by $\lambda_{\rm FH}$ (the subscript$_{\rm FH}$ stands for fundamental harmonic), goes approximately from 1561 to 1566 nm that is equivalent to a bandwidth of $\sim$620 GHz. Although this bandwidth is smaller than assigned for the interacting signals, the actual limitation on the phase comparator resides on the SF components that will be generated. Since SHG is a particular case of SF generation when the optical frequencies to be summed are equal, one must ensure that the central wavelengths of the data signal and optical clock are such that their SF wavelength matches $\lambda_{\rm SH}$. In other words, $\lambda_{\rm SF}$ will take the same values as $\lambda_{\rm SH}$ does in Fig. 3, so now the wavelength ranges satisfying (2) are within the transparency range of the material from $\sim$0.35 to $\leq$ 4 μm [24], which are larger than $\lambda_{\rm FH}$'s range for SHG. The SF components must be limited to fall within a 1 nm window either at $\lambda_{\rm SH}\sim$781.5 nm or at $\lambda_{\rm SH}\sim$782.5 nm for maximum SF-generation conversion efficiency, otherwise no SF components will be generated.

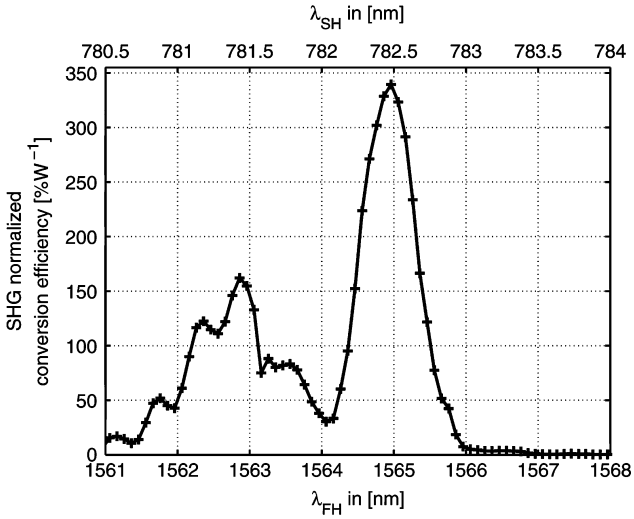

Fig. 3. Experimental second harmonic generation (SHG) tuning curve for the ARW–PPLN device. The bottom and top axes represent, respectively, the wavelengths at the input and output of the device. FH: Fundamental harmonic; SH: Second harmonic.

To illustrate this, we refer to Fig. 4 taking as an example the particular case when the modulation frequency for the input signal is about 4 times that of the optical clock, in such a way, the harmonic at the modulation frequency of the former interacts with the 4th harmonic of the latter, producing a slight frequency detuning; $|f_{\rm s}-4f_{\rm c}|$. In the figure, we can observe that the spectral components at $\lambda_{\rm s}$ and $\lambda_{\rm c}$ interact pairwise, generating their optical sum-frequency indicated in the gray region (the SF bandwidth of the PPLN); the central lines create an SF central peak at $\lambda_{\rm SF}$, whereas the lateral lines or harmonics of the respective modulation frequencies, denoted by $\Delta\lambda_{\rm s} = (\lambda_{\rm s}^2/c)\Delta f_{\rm s}$ and $\Delta\lambda_{\rm c} = (\lambda_{\rm c}^2/c)\Delta f_{\rm c}$, where c is the speed of light and Δf_i ($i =_{\rm s}$ and $_{\rm c}$) is the frequency range between harmonics, generate SF peaks around $\lambda_{\rm SF}$. If the detuning frequency $|f_{\rm s} - 4f_{\rm c}|$ is reduced to zero, the generated peaks will be moved toward the central one, otherwise they will move away from it being attenuated by the filter function of the PPLN.

B. Error Signals

The experimental setup used to demonstrate the phase comparator operation is illustrated in Fig. 5. The data signal is generated by an erbium-glass oscillator pulse-generating laser (ERGO-PGL) at 9.953175 GHz tuned to 1558.85 nm. The pulses are on-off-keying (OOK) modulated with a selected pseudorandom bit sequence (PRBS) and subsequently multiplexed up to 40 Gbit/s. Afterward, they are chirped, compressed, and multiplexed up again to reach 160, 320, and 640 Gbit/s. The optical clock tuned to 1565.9 nm, consists of 10 GHz pulses from a tunable mode-locked laser driven by a VCO. The pulses are then amplified by a semiconductor optical amplifier (SOA) and passed to a pulse compressor stage, based on soliton compression, in order to resolve the input-signal pulses. The input signal and the optical clock are coupled into

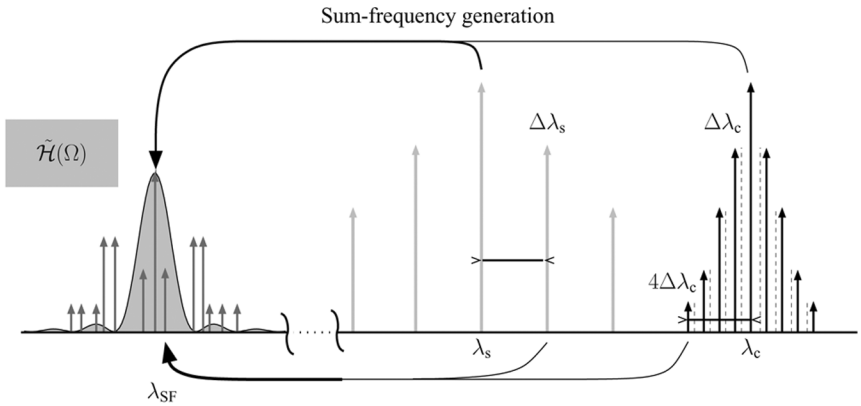

Fig. 4. Illustration of the TWM component generation process. The spectral components of λ_s and λ_c interact pairwise generating their optical SF; the central lines create an SF central peak at λ_{SF}, whereas the lateral lines create SF component peaks around the central one. If the detuning frequency $|f_s - 4f_c|$ is null, the lateral SF components will be displaced to the central peak. A QPM condition $\Delta k_Q = 0$ is considered.

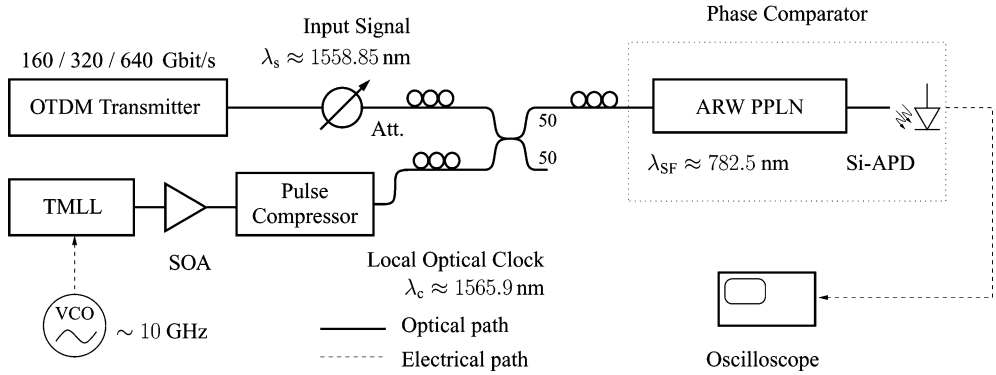

Fig. 5. Experimental setup to demonstrate the phase comparator operation. The phase comparator produces an error signal corresponding to the phase difference between the input signal and the local optical clock. TMLL: tunable mode-locked laser; SOA: semiconductor optical amplifier; Si-APD: silicon avalanche-photodetector; VCO: voltage-controlled oscillator.

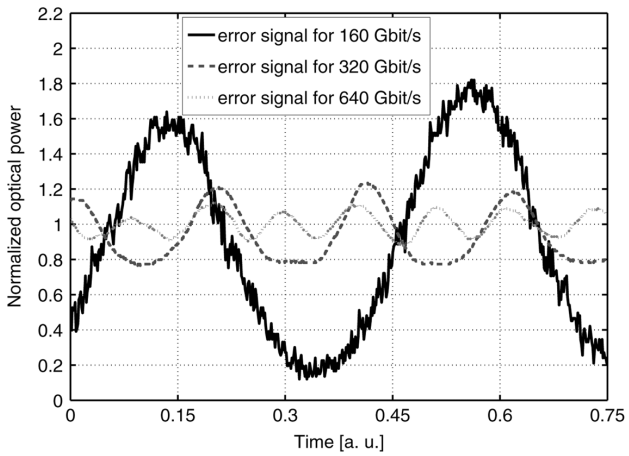

Fig. 6. Error signals produced by the phase comparator at different bit rates of the input signal. These error signals are the result of the interaction between the input signal and the respective lth harmonic of the local optical clock at a particular bit-rate. Bit-rate, kth harmonic: 160 Gbit/s, $l = 16$; 320 Gbit/s, $l = 32$; 640 Gbit/s, $l = 64$.

the ARW–PPLN device, generating through SF, an error signal at a wavelength about 781.5 nm. The error signal, bearing information about the phase difference between the envelopes of the interacting signals, is detected by a silicon avalanche photodetector (APD).

Fig. 6 shows experimental traces of the error signal produced by the phase comparator corresponding to different bit rates of the input signal. The error signals were normalized with respect to their average optical power P_0. These traces can also be interpreted as the time correlation between the pulses of the input and the optical clock.

For the 160 Gbit/s and 320 Gbit/s experiments, the input and the optical clock pulses widths, measured with an optical correlator, were 1.8 ps at full width at half-maximum (FWHM) and 2.7 ps FWHM, respectively. In this case, the optical clock pulses were not compressed, and the PRBS selected for the data signal was $2^7 - 1$. The respective average optical power injected into the ARW–PPLN device was 2.4 dBm for the input signal and -3.8 dBm for the optical clock.

As for the 640 Gbit/s experiment, the bit-rate limitation is determined by the pulse width of the optical clock and the temporal resolution intrinsic to the ARW–PPLN device. Thus, it was necessary to compress the pulses. For these bit rates, the pulses widths were $\simeq 560$ fs FWHM for the input data signal and $\simeq 760$ fs FWHM for the optical clock with an average optical power of 16.5 dBm and -4 dBm, respectively. The available dynamic power range for the data input signal in the experiment was about 18 dB. 16.5 dBm being the upper limit and -1.5 dBm the lower limit. The upper limit was imposed by the available amplification gain in the experiment.

The PRBS selected for the data input was $2^{15} - 1$. The error signal traces show that the pulses are well resolved, presenting a modulation index (contrast) about 80% for the 160 Gbit/s error

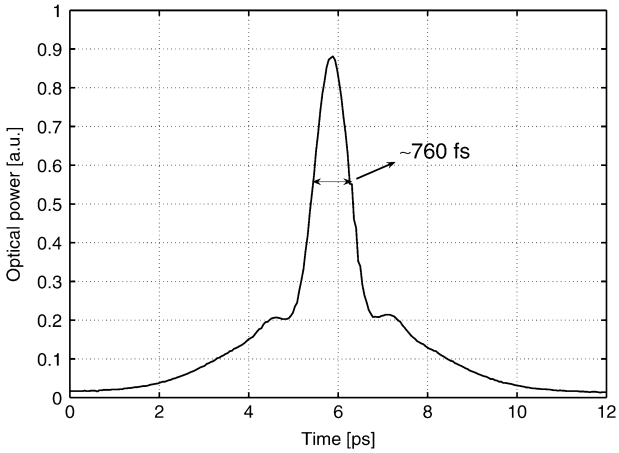

Fig. 7. Optical clock pulses width measured with an optical correlator. Pulse width ~ 760 fs with a pedestal amplitude about 20% of the peak power.

signal case, whereas 20% and 10% for the 320 and 640 Gbit/s error signal cases, respectively. We believe this low contrast is caused by a contribution to the average optical power due to: 1) the SHG of the interacting signals within the range of 1561–1566 nm; 2) the SF generation among the different combinations of wavelengths between the interacting signals that match (2); and 3) the optical clock pulses pedestals, whose magnitude corresponds to about 20% of the pulse peak optical power (Fig. 7). Although the modulation indices are relatively low when compared to the one obtained in the 160 Gbit/s error signal case, the error signals are suitable for the OEPLL to lock onto the data input signal.

C. Optical Spectra

As depicted in Fig. 8(a), the spectrum of a 640 Gbit/s OTDM signal (black curve) traced alongside to that of the optical clock (gray curve), corresponds to the measured spectrum at the input of the ARW–PPLN device, whereas Fig. 8(b) illustrates the measured spectrum at its output.

Since the interacting signals hold a wide spectral content, the effect of SHG and SF generation produced by the interaction not only between the data input signal and the optical clock but also by the interacting signals with themselves is superposed on one another as illustrated in Fig. 8(b) where two regions, denoted by TWM1 and TWM2, represent each the combined effect. TWM1 represents the combined effect within the range between 780.5 and 782 nm, while TWM2 is within the range between 782 and 783 nm.

The peak at $\lambda_{\mathrm{SF}} \simeq 781.2$ nm is produced by the interaction between the discrete spectral components at the central wavelengths of interacting signals. Their respective values, $\lambda_{\mathrm{s}} = 1558.85$ nm and $\lambda_{\mathrm{c}} = 1565.9$ nm when plugged into (2), verify the wavelength at which the peak is present. Moreover, we verify that the wavelengths of the discrete components corresponding to the spectral lines at 640 GHz ($\sim \pm 5.2$ nm to the central wavelength) of the interacting signals also contribute to the process of creation of the peak present in TWM1. Inserting the values of: i) $\lambda_{\mathrm{s}} \simeq 1564$ nm/$\lambda_{\mathrm{c}} \simeq 1560.80$ nm; or ii) $\lambda_{\mathrm{s}} \simeq 1553.55$ nm/$\lambda_{\mathrm{c}} \simeq 1571.35$ nm into (2), match the wavelength at which the peak is present.

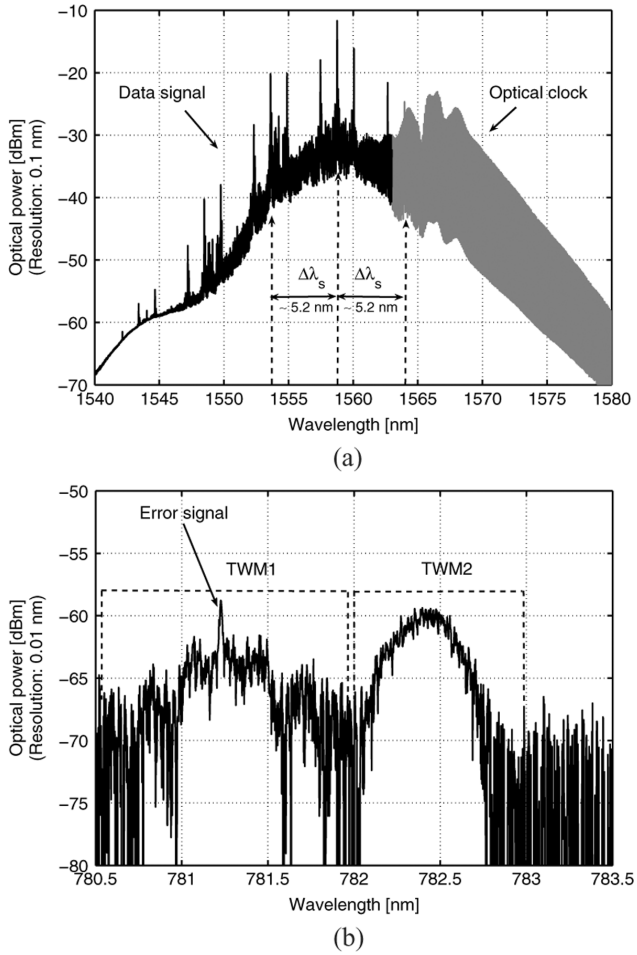

Fig. 8. (a) Optical spectrum of a 640 Gbit/s OTDM signal (black curve) traced alongside to that of the optical clock (gray curve). Spectrum measured at the input of the ARW–PPLN device. (b) Combined effect of SHG and SF generation between the interacting signals. Spectrum measured at the output of the ARW–PPLN device. (a) Optical spectrum at the input of the ARW–PPLN. (b) Optical spectrum at the output of the ARW–PPLN.

Furthermore, if residual peaks at the spectral lines associated with the subharmonics of the 640 Gbit/s data signal are ever present, they will also participate in the peak-creation process in the TWM1 section only if the associated wavelengths with theses spectral lines match (2). The peaks closer to 480 GHz ($\sim \pm 3.8$ nm to the central wavelength) and 160 GHz ($\sim \pm 1.3$ nm to the central wavelength) present in the input signal are due to irregular optical-phase correlation among the OTDM channels, which might have been produced by temperature drifts in the planar-lightwave circuit (PLC)-based OTDM multiplexer during measurements. On the other hand, the regularity of the error signal in the 640 Gbit/s configuration invites us to formulate the hypothesis that a reduction of residual peaks in the OTDM signal was achieved since the fundamental harmonic of the error signal in question is stronger than its subharmonic or higher harmonics.

Another additional property drawn from Fig. 8(b) is that no amplified spontaneous emission (ASE) is present given that

TWM is a coherent process where the phase of the electrical fields match each other in order to interfere constructively and buildup a particular interaction.

D. Group-Velocity Mismatch

The GVM intrinsic to the ARW–PPLN device, estimated to be of the order of $\delta_v = 0.29$ ps/mm, does not represent a critical issue for the pursued application because of the low-frequency variation of the error signal. In other words, if interest is paid in applications concerning wavelength conversion of short optical pulses to its SHG, the effect of walkoff between the pulses at FH and SHG must be considered. If it is not, this implies a reduced SHG efficiency, waveform distortion, and broadening of the generated pulses. So that, the GVM parameter sets the limit for the maximum allowed interaction distance over which the FH and SHG pulses walk off. The latter, known as group-velocity walk-off length [27], $L_{\rm gv} = \Delta t/|\delta_v|$, where Δt is the FH pulse width, avoids successive SHG pulses overlap. For example, a pulse width of the order of 3 ps, typical for applications at 160 Gbit/s, requires the accumulated walkoff time to be limited to less than $\Delta t = 3.65$ ps. Therefore, the maximum allowed interaction distance must be less than $L_{\rm gv} = 12.6$ mm, otherwise SHG pulses longer than 6.25 ps will result. The device employed in our experiments holds an accumulated walkoff time of $\sim$8.7 ps, a value which is large, for example, for SHG of a stream of optical pulses at 160 Gbit/s. On the other hand, the walkoff between the interacting signals and its SF generation at the frequency of the error signal is not considerably meaningful. Furthermore, since TWM is an ultrafast phenomenon, high resolution to resolve the pulses of a 640 Gbit/s OTDM signal, as shown in Fig. 6, is exhibited.

According to [28], [29], it is possible to conceive ARW–PPLN devices with GVMs as low as $\sim$3 fs/mm by means of tailoring the off-diagonal nonlinear optical coefficient d_{32}, which is translated into an enlargement of the PPLN tuning curve, allowing for wavelength conversion applications of optical short pulses beyond 160 Gbit/s. For a GVM of 3 fs/mm in a waveguide length of 15 mm, the PPLN tuning curve would reach the $\sim$50 nm width.

V. OEPLL's Transfer Function

The interest of the section is demonstrating how the $\chi^{(2)}$ phase comparator's sensitivity is derived and incorporated to the transfer function (TF) of a PLL in order to obtain that of an OEPLL. The modified TF can be used for performance assessment of the loop as a CR unit.

A. Phase Comparator Sensitivity

As indicated in several [30]–[33], each element the PLL is composed of has an associated sensitivity that takes part in the gain of the loop; a parameter that helps us to quantify the loop bandwidth and the amount of phase noise transferred to its output (the recovered clock). Furthermore, when new elements replace the existing ones, their sensitivity must be derived in order to estimate such gain. For the $\chi^{(2)}$ phase comparator, the following procedure is applied.

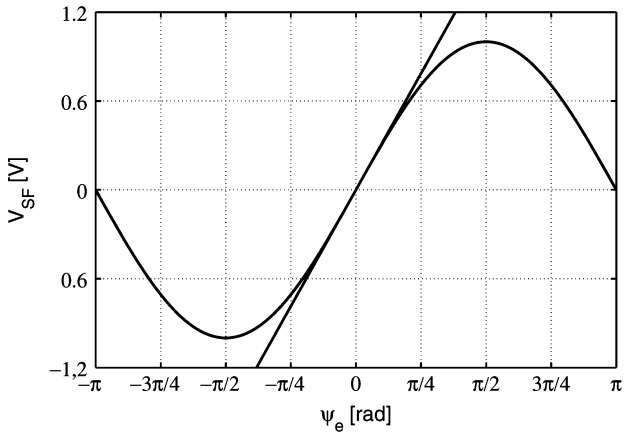

Fig. 9. Usable region of the phase comparator. The range within the which the phase comparator operation is considered linear is $\pm\pi/4$ in the vicinity of $\Psi_e = 0$.

As demonstrated in [30], when the PLL is locked there is a relative phase difference of $\pi/2$ between the local oscillator and the input signal; the quadrature condition. Applying this argument to the OEPLL case, we can make the following substitutions: $\Phi_1 = N\varphi_1$ and $\Phi_2 = N\varphi_2 + \pi/2$, where Φ_2 is the phase at the output of the optical clock when both the phase quadrature and the locked condition are fulfilled, so (8) becomes

$$P_{\rm SF} = P_0 + P_1 \sin[\Phi_1 - \Phi_2] \tag{10}$$

where we have neglected the higher order terms. The usable range, where the phase comparator operation is approximately linear, is limited to within $\pm\pi/4$ about $\Psi_e = \Phi_1 - \Phi_2 = 0$ (Fig. 9), yielding a phase detector range of $\pi/2$. Thus, in this range of detection (10) becomes

$$V_{\rm SF} = \mathcal{R}P_0 + \mathcal{R}P_1\Psi_e \tag{11}$$

where $\mathcal{R}$ is the sensitivity of the APD given in units of V/W. To determine the phase comparator sensitivity, denoted by $K_{\rm PPLN}$ (in units of V/rad), we take the derivative of $V_{\rm SF}$ respect to φ_e, the phase error at the scale of the OTDM signal base rate, that is

$$K_{\rm PPLN} = \left|\frac{dV_{\rm SF}}{d\Psi_e}\cdot\frac{d\Psi_e}{d\varphi_e}\right| = N\mathcal{R}P_1 \tag{12}$$

where N is the factor by which $f_{\rm c}$ is scaled to be proportional to $f_{\rm s}$. In other words, since the output of the OEPLL consists of a synchronized signal of frequency $f_{\rm s}/N$, every change in its phase or frequency is scaled by N in order to be proportional to the rate frequency $f_{\rm s}$ at which the phase comparison takes place.

B. Overall Transfer Function

The filter was designed so that the OEPLL in question is described by a second-order TF. According to [30], the OEPLL TF can be derived by using the diagram shown in Fig. 1 and

by applying Laplace-domain analysis. The TF, denoted by $H_{\mathrm{OEPLL}}(s)$, is thus given by

$$H_{\mathrm{OEPLL}}(s) = \frac{s(2\zeta\omega_n - \omega_n^2/K) + \omega_n^2}{s^2 + 2\zeta\omega_n s + \omega_n^2} \tag{13}$$

where ω_n, ζ, and K designate the natural frequency (in rad/s), the damping coefficient (dimensionless) and the gain of the loop (in Hz), respectively. These parameters, related to the time constants of the filter and the gain of the loop, are used to describe the transient and steady state response of a feedback system [34]. For this particular system, these parameters are given by

$$K = K_{\mathrm{VCO}} K_1 K_2 K_{\mathrm{PPLN}} \tag{14a}$$

$$\omega_n = \sqrt{\frac{K}{T}} \tag{14b}$$

$$\zeta = \frac{T_2 \omega_n}{2} \tag{14c}$$

where T_2, T, K_2, and K_1 define the time constants and dc gain of the filter and amplifier, respectively. Finally, the variable K_{VCO} represents the sensitivity associated with the VCO and K_{PPLN} the sensitivity associated with the $\chi^{(2)}$ phase comparator.

VI. Conclusion

A novel application of a $\chi^{(2)}$ nonlinear optical device was demonstrated. The application consisted in an ultrafast phase comparator incorporated into a PLL to allow clock recovery of ultrahigh-speed OTDM signals. The ARW–PPLN device employed to demonstrate this application shows sufficient high temporal resolution to resolve the optical pulses of a 640 Gbit/s OTDM signal. Since the error signal presents a low-frequency variation, the GVM parameter intrinsic to the ARW–PPLN is not a critical issue for the pursued application. TWM processes performed in PPLN devices do not generate ASE; hence, PPLN does not contribute to noise in the loop. The $\chi^{(2)}$ phase comparator's sensitivity was determined and incorporated into the OEPLL's gain. We believe that ARW–PPLN devices are strong candidates for implementation into ultrahigh-speed CR future systems.

References

[1] S. Kawanishi and M. Saruwatari, "Ultra-high-speed PLL-type clock recovery circuit based on all-optical gain modulation in traveling-wave laser diode amplifier," *J. Lightw. Technol.*, vol. 11, no. 12, pp. 2123–2129, Dec. 1993.

[2] O. Kamatani and S. Kawanishi, "Ultra-high speed clock recovery with phase lock loop based on four-wave mixing in a traveling-wave laser diode amplifier," *J. Lightw. Technol.*, vol. 14, no. 8, pp. 1757–1767, Aug. 1996.

[3] O. Kamatani and S. Kawanishi, "Prescaled timing extraction from 400 Gb/s optical signal using a phase lock loop based on four-wave-mixing in a laser diode amplifier," *IEEE Photon. Technol. Lett.*, vol. 8, no. 8, pp. 1094–1096, Aug. 1996.

[4] L. K. Oxenløwe, P. Jeppesen, D. Zibar, M. Galili, A. T. Clausen, and L. J. Christiansen, "Clock recovery for 320 Gb/s OTDM data using filtering-assisted XPM in an SOA," presented at the CLEO/Europe, Munich, Germany, Jun. 2005, (CI3-4-MON).

[5] H. C. H. Mulvad, E. Tangdiongga, H. de Waardt, and H. J. S. Dorren, "40 GHz clock recovery from 640 Gbit/s OTDM signal using SOA-based phase comparator," *Electron. Lett.*, vol. 44, no. 2, pp. 146–147, Jan. 2008.

[6] D. T. K. Tong, K.-L. Deng, B. Mikkelsen, G. Raybon, K. F. Dreyer, and J. E. Johnson, "160 Gbit/s clock recovery using electroabsorption modulator-based phase-locked loop," *Electron. Lett.*, vol. 36, no. 23, pp. 1951–1952, Nov. 2000.

[7] J. P. K. Turkiewicz, E. Tangdiongga, G. D. Khoe, and H. de Waardt, "Clock recovery and demultiplexing performance of 160 Gb/s OTDM field experiments," *IEEE Photon. Technol. Lett.*, vol. 16, no. 6, pp. 1555–1557, Jun. 2004.

[8] R. Salem, G. E. Tudury, T. U. Horton, G. M. Carter, and T. E. Murphy, "Polarization-insensitive optical clock recovery at 80 Gb/s using a silicon photodiode," *IEEE Photon. Technol. Lett.*, vol. 17, no. 9, pp. 1968–1970, Sep. 2005.

[9] E. S. Awad, P. K. Cho, N. Moulton, and J. Goldhar, "Subharmonic optical clock recovery from 160 Gb/s using time-dependent loss saturation inside a single electroabsorption modulator," *IEEE Photon. Technol. Lett.*, vol. 15, no. 12, pp. 1764–1766, Dec. 2003.

[10] E. Tangdiongga, J. P. K. Turkiewicz, G. D. Khoe, and H. de Waardt, "Clock recovery by a fiber ring laser employing a linear optical amplifier," *IEEE Photon. Technol. Lett.*, vol. 16, no. 2, pp. 611–613, Feb. 2004.

[11] C. Ware, L. K. Oxenløwe, F. Gómez Agis, H. C. H. Mulvad, M. Galili, S. Kurimura, H. Nakajima, J. Ichikawa, D. Erasme, A. T. Clausen, and P. Jeppesen, "320 Gbps to 10 GHz sub-clock recovery using a PPLN-based opto-electronic phase-locked loop," *Opt. Exp.*, vol. 16, no. 7, pp. 5007–5012, Mar. 2008.

[12] L. K. Oxenløwe, F. Gómez Agis, C. Ware, S. Kurimura, H. C. H. Mulvad, M. Galili, K. Kitamura, H. Nakajima, J. Ichikawa, D. Erasme, A. T. Clausen, and P. Jeppesen, "640 Gbit/s data transmission and clock recovery using an ultrafast periodically poled lithium niobate device," in *Proc. Opt. Fiber Commun. Conf.*, San Diego, CA, Feb. 23–28, 2008, postdeadline papers, paper PDP22.

[13] L. K. Oxenløwe, F. Gómez Agis, C. Ware, S. Kurimura, H. C. H. Mulvad, M. Galili, K. Kitamura, H. Nakajima, J. Ichikawa, D. Erasme, A. T. Clausen, and P. Jeppesen, "640 Gbit/s clock recovery using periodically poled lithium niobate," *Electron. Lett.*, vol. 44, no. 5, pp. 370–371, Mar. 2008.

[14] C. Langrock, S. Kumar, J. E. McGeehan, and M. M. Fejer, "All-optical signal processing using $\chi^{(2)}$ nonlinearities in guided-wave devices," *J. Lightw. Technol.*, vol. 7, no. 24, pp. 2579–2592, Jul. 2006.

[15] J. E. McGeehan, M. Giltrelli, and A. E. Willner, "All-optical digital 3-input and gate using sum- and difference-frequency generation in a PPLN waveguide," in *Dig. LEOS Summer Topical Meetings*, Munich, Germany, Jul. 2005, pp. 179–180.

[16] T. Ohara, H. Takara, I. Shake, K. Mori, S. Kawanishi, S. Mino, T. Yamada, M. Ishii, T. Kitoh, T. Kitagawa, K. R. Parameswaran, and M. M. Fejer, "160-Gb/s optical-time division multiplexing with PPLN hybrid integrated planar lightwave circuit," *IEEE Photon. Technol. Lett.*, vol. 15, no. 2, pp. 302–304, Feb. 2003.

[17] J. Huang, C. Langrock, X. P. Xie, and M. M. Fejer, "Monolithic 160 Gbit/s optical time-division multiplexer," *Opt. Lett.*, vol. 32, no. 16, pp. 2420–2422, Aug. 2007.

[18] D. Caccioli, A. Paoletti, A. Schiffini, A. Galtarossa, P. Griggio, G. Lorenzetto, P. Minzioni, S. Cascelli, M. Guglielmucci, L. Lattanzi, F. Matera, G. M. Tosi Belefi, V. Quiring, W. Sohler, H. Suche, S. Vehovc, and M. Vidmar, "Field demonstration of in-line all-optical wavelength conversion in a WDM dispersion managed 40-Gbit/s link," *IEEE J. Sel. Topics Quantum Electron.*, vol. 10, no. 2, pp. 356–362, Mar./Apr. 2004.

[19] P. Minzioni, I. Cristiani, V. Degiorgio, L. Marazzi, M. Martinelli, C. Langrock, and M. M. Fejer, "Experimental demonstration of nonlinearity and dispersion compensation in an embedded link by optical phase conjugation," *IEEE Photon. Technol. Lett.*, vol. 18, no. 9, pp. 995–997, May 2006.

[20] S. L. Jansen, D. van den Borne, P. M. Krummrich, S. Spalter, G.-D. Khoe, and H. de Waardt, "Long-haul DWDM transmission systems employing optical phase conjugation," *IEEE J. Sel. Topics Quantum Electron.*, vol. 12, no. 4, pp. 505–520, Jul./Aug. 2006.

[21] Y. Nishida, H. Miyazawa, M. Asobe, O. Taganaga, and H. Susuki, "0-dB wavelength conversion using direct-bonded QPM-Zn:$LiNbO_3$ ridge waveguide," *J. Lightw. Technol.*, vol. 17, no. 5, pp. 1049–1051, Jul. 2005.

[22] S. Kurimura, Y. Kato, M. Maruyama, Y. Usui, and H. Nakajima, "Quasi-phase-matched adhered-ridge-waveguide in $LiNbO_3$," *Appl. Phys. Lett.*, vol. 89, no. 19, pp. 1123-1–1123-3, 2006.
[23] F. Gómez-Agis, C. Ware, D. Erasme, R. Ricken, V. Quiring, and W. Sohler, "10-GHz clock recovery using an opto-electronic phase-locked loop based on three-wave mixing in periodically-poled lithium niobate," *IEEE Photon. Technol. Lett.*, vol. 18, no. 13, pp. 1460–1463, Jul. 2006.
[24] L. E. Myers, R. C. Eckardt, M. M. Fejer, R. L. Byer, W. R. Bosenberg, and J. W. Pierce, "Quasi-phase-matched optical parametric oscillators in bulk periodically poled $LiNbO_3$," *J. Opt. Soc. Am. B*, vol. 12, no. 11, pp. 2102–2116, Nov. 1995.
[25] M. M. Fejer, G. A. Magel, D. H. Junt, and R. L. Byer, "Quasi-phase matching second harmonic generation: Tuning and tolerances," *IEEE J. Quantum Electron.*, vol. 28, no. 11, pp. 2631–2653, Nov. 1992.
[26] Y. Fukuchi, T. Sakamoto, K. Taira, K. Kikuchi, D. Kunimatsu, A. Suzuki, and H. Ito, "Speed limit of all-optical gate switches using cascaded second-order nonlinear effect in quasi-phase-matched $LiNbO_3$ devices," *IEEE Photon. Technol. Lett.*, vol. 14, no. 9, pp. 1267–1269, Sept. 2002.
[27] G. Imeshev, M. A. Arbore, M. M. Fejer, A. Galvanauskas, M. Fermann, and D. Harter, "Ultrashort-pulse second-harmonic with longitudinally nonuniform quasi-phase-matching gratings: Pulse compression and shaping," *J. Opt. Soc. Am. B*, vol. 17, no. 2, pp. 304–318, Feb. 2000.
[28] N. E. Yu, J. H. Ro, M. Cha, S. Kurimura, and T. Taira, "Broadband quasi-phase-matched second-harmonic generation in MgO-doped periodically poled $LiNbO_3$ at the communications band," *Opt. Lett.*, vol. 27, no. 12, pp. 1046–1048, Jun. 2002.
[29] N. E. Yu, S. Kurimura, K. Kitamura, J. H. Ro, M. Cha, S. Ashihara, T. Shimura, K. Kuroda, and T. Taira, "Efficient frequency doubling of a femtosecond pulse with simultaneous group-velocity and quasi-phase-matching in periodically poled MgO-doped lithium niobate," *Appl. Phys. Lett.*, vol. 82, no. 20, pp. 3388–3390, May 2003.
[30] A. Blanchard, *Phase-Locked Loops: Application to Coherent Receiver Design*. Hoboken, NJ: Wiley, 1976.
[31] F. M. Gardner, *Phaselock Techniques*, 3rd ed. Hoboken, NJ: Wiley, 2005.
[32] G. Nash, "Phase-locked loop design fundamentals," Motorola, Appl. Note AN535, Feb. 1994.
[33] A. W. Moore, "Phase-locked loops for motor-speed control," *IEEE Spectrum*, vol. 10, pp. 61–67, Apr. 1973.
[34] K. Ogata, *Modern Control Engineering*, 2nd ed. Englewood Cliffs, NJ: Prentice-Hall, 1990.

Fausto Gómez-Agis was born in México D.F., México, in 1975. He received the B.Sc. degree in electronics from the Instituto Tecnológico de Mazatlán, Sinaloa, México, in 1996, and the M.Sc. degree in optics from CICESE Research Center, Ensenada B.C., México, in 1999. He is currently working toward the Ph.D. degree in the Department of Communications and Electronics at École Nationale Supérieure des Télécommunications (now TELECOM ParisTech), Paris, France.

In 2000, he joined the Last-Mile Access Department of TELMEX (Teléfonos de México), Jalisco, México, as a Systems Engineer. From 2001 to 2004, he joined CIDEC (CONDUMEX R&D Center), Querétaro, México, where he was involved with research activities on plastic optical fiber communications such as design, construction and evaluation of devices for Fast-Ethernet LAN applications. He is currently involved in research on optoelectronic clock recovery.

Leif Katsuo Oxenløwe received the B.Sc. degree in physics and astronomy from the Niels Bohr Institute, University of Copenhagen, Copenhagen, Denmark, in 1996. In 1998, he received the International Diploma of Imperial College of Science, Technology and Medicine, London, U.K., and the M.Sc. degree from the University of Copenhagen. He received the Ph.D. degree from the Technical University of Denmark, Lyngby, Denmark, in 2002.

In May 2004, he joined and managed the project ULTRA-NET funded by the Danish Research Council. In August 2007, he embarked on the project NANO-COM also funded by the Danish Research Council, and this project deals with nanotechnology-based solutions for ultrahigh-bit-rate communications. He is currently an Associate Professor at DTU Fotonik, Department of Photonics Engineering, Technical University of Denmark, where he is the group leader of the Ultra-High-Speed Optical Communications group. He is working with experimental research in the field of ultrafast optical communications (above 160 Gb/s). He has been working within the EU IST project TOPRATE, and the Danish research council financed project SCOOP. He has authored or co-authored more than 110 peer-reviewed publications.

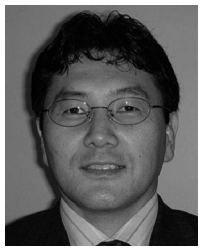

Sunao Kurimura received the B.D. and M.D. degrees in physics in 1988 and 1990, respectively, and the Ph.D. degree in engineering in 1997, all from Waseda University, Tokyo, Japan.

He joined Fujitsu Laboratories, Inc. as a Researcher in 1990. After working three years with Fujitsu, he returned to Waseda University. He was a Visiting Scholar at Stanford University, Stanford, CA, from 1997 to 1999 and joined the Institute for Molecular Science in 1999. Since 2001, he has been with the National Institute for Materials Science, Ibaraki, Japan, as a Senior Researcher. He is currently with Waseda University and Kyusyu University, Japan, as an Associate Professor. His interest ranges from material science to optoelectronics and currently focuses on nonlinear optical bulk and waveguide devices.

Dr. Kurimura received the Funai Promotion Award for Information Technology in 2008.

Cédric Ware was born in Paris, France, on January 24, 1977. He received the B.Sc. degree in computer science and the M.Sc. degree in physics from the École Normale Supérieure, Paris, and the Université Paris 6 and 7, Paris, in 1996, and the Engineering degree from the École Nationale Supérieure des Télécommunications, Paris, in 1998, where he also received the Ph.D. degree, specializing in optoelectronic clock recovery, in 2003.

Since 1998, he has been with the Department of Communications and Electronics, École Nationale Supérieure des Télécommunications (now TELECOM ParisTech), as an Assistant Professor, and has been an Associate Professor since 2007. He is a national Delegate for the European Cooperation in the Field of Scientific and Technical Research (COST) 288 on nanoscale and ultrafast photonics and the Vice Chairman of its working group on photonics devices. He also participates in COST 291 on digital optical networks and the European Networks of Excellence BONE and EuroFOS. His current research activities include optical signal processing for use in optical communications networks, notably clock recovery, packet label recognition, and optical code division multiple access.

Dr. Ware is a member of the Optical Society of America.

Hans Christian Hansen Mulvad (S'07–A'08) was born in Copenhagen, Denmark, in 1976. He received the M.Sc. degree in physics from the University of Copenhagen, Copenhagen, Denmark, in 2004. He is currently working toward the Ph.D. degree in the Department of Communications, Optics and Materials, Technical University of Denmark, Lyngby, Denmark.

He is currently involved in research on fiber nonlinearities for high-speed signal processing.

Michael Galili was born in Aabenraa, Denmark, in 1977. He received the M.Eng. degree in applied physics from the Technical University of Denmark, Lyngby, Denmark, in 2003, and the Ph.D. degree in optical communications and signal processing from the Communications Optics and Materials Department, Technical University of Denmark, in 2007. He is currently a Postdoctoral Researcher at the Technical University of Denmark.

He is the author or co-author of more than 40 peer-reviewed scientific publications. His current research interests include optical signal processing of high-speed optical data signals.

Didier Erasme was born in Paris, France, in 1960. In 1983, he received a diplôme d'Ingénieur in physical engineering from the École Nationale Supérieure d'Ingénieurs Electriciens de Grenoble (INPG). In 1987, he received the Ph.D. degree on LiNbO3 high-frequency integrated-optic modulators in the Electrical and Electronic Engineering Department, University College London (UCL), London, U.K.

After a two-year postdoctoral work on electrooptic sampling of GaAs integrated circuits at UCL, he joined the École Nationale Supérieure des Télécommunications (Télécom ParisTech) in 1990 as an Associate Professor in optoelectronic. In 1995, he obtained a Habilitation à diriger des recherches. He spent a six-month sabbatical in Prof. M. Smit's group in Delft University, Delft, The Netherlands. He has been a full Professor since 1998. He is an author or co-author of more than 70 publications and communications in international journals and conferences. He has participated in the European programmes OPTIMIST and BREAD dedicated to the road-mapping of European Broadband-for-all activities in Europe and to the European Network of Excellence ePhoton/ONe and now BONE and EUROFOS. His current research interests are in the area of new optical functions for telecommunication optical systems and networks. Particularly, he has developed a strong interest in semiconductor laser amplifiers and other nonlinear optical devices for applications in all-optical signal processing. Applications range from ultra high-speed clock recovery and OTDM demultiplexing to the realization of subsystems dedicated to optical packet switching nodes.